Impact of mathematical correlations on the statistic of the congruency test case study: B-splines surface approximation from bridge observations

Kermarrec Gaël[1], Alkhatib Hamza[1], Bureick Johannes[1], Kargoll Boris[1]

[1] Geodetic Institute, Leibniz Universität Hannover, Nienburger Str. 1, 30167 Hannover, Germany, (kermarrec@gih.uni-hannover.de, alkhatib@gih.uni-hannover.de, bureick@gih.uni-hannover.de, kargoll@gih.uni-hannover.de)

Key words: *B-spline, Terrestrial Laser Scanner, congruency test, mathematical correlations, heteroscedasticity*

ABSTRACT

B-spline surfaces possess attractive properties such as a high degree of continuity, which is important for computing curvature. Since the local support of the basis functions allows to control the shape of the estimated surface, they are increasingly used in the field of geodesy, where their main application is the fitting of surfaces to, e.g., 3D point clouds obtained from terrestrial laser scanners (TLS). By comparing different epochs, deformation can be detected more easily for nearly all kind of objects by using test statistics such as the congruency test.

The concept of surface approximation is similar to a regression problem where the model is the surface representation and the data are the sampled points on the surface. Consequently, besides improving the functional model with new strategies to determine the knot vector, the stochastic model of the underlying observations has to be correctly specified. Otherwise, biases in test statistics are unavoidable and compromise the detection of small deformations when the congruency test is used. Unfortunately, measurements from TLS are not as simple as point clouds for Computer Aided Graphics: the raw observations are not directly Cartesian coordinates but polar coordinates, i.e. range and angles, which additionally possess different variances. A transformation from polar to Cartesian coordinates is mandatory to determine the weighting functions or control points of the B-splines approximation by a least-squares adjustment. Mathematical correlations are thus introduced in the already heteroscedastic transformed observations. As they lead to fully populated variance covariance matrices, they remain mostly neglected and an oversimplified stochastic model is used assuming homoscedasticity and independency of the transformed observations. In this contribution, the impact of neglecting mathematical correlations in deformation analysis with the congruency test will be studied. It will be shown that these correlations can eventually be reduced to an inflation variance factor, which allows for their simplified handling in matrix products. In a case study with real data from a bridge under loading, the impact of neglecting them will be investigated, highlighting in which cases considering mathematical correlations in the congruency test is necessary or not for a trustworthy deformation detection. Heteroscedasticity will be taken into consideration using an intensity-based model accounting for geometry and object properties.

I. INTRODUCTION

One of the key problems of civil engineering is the detection of a structure's deformation to identify damages and to avoid tragic experiences of a total collapse of a bridge (Gumus *et al*. 2013). As they can acquire three-dimensional high-density point clouds of nearly every object quickly and without complex and expensive surveying methods, terrestrial laser scanners (TLS) have gained an increased interest for deformation analysis applications, see e.g. Xu *et al*. (2018), Yang *et al*. (2017), Pesci *et al*. (2013). Deformations can be detected with specific software by comparing directly the point clouds taken at different epochs, provided that an accurate registration is performed (Paffenholz and Bae 2012). However, the impact of outliers, errors and scattering is not considered in this direct approach. Another possibility is thus to mathematically approximate the scanned surfaces and to compare the approximations obtained at different epochs, by accounting for the measurements' uncertainties. Because it is a flexible method, surface approximation using B-splines is becoming more and more popular in the field of geodesy (Bureick *et al*. 2016). Indeed, the restriction due to the use of geometrical primitives such as circles, planes and cylinders with the Gauss-Helmert Model (cf. Lenzmann and Lenzmann 2004) is avoided. Nearly every object can be approximated with B-

splines, and improvements e.g. with respect to the determination of the knot vector remain an active field of research (Piegl and Tiller 1997, Gálvez *et al*. 2015, Bureick *et al*. 2016). Using this regression splines approach, the so-called control points (CP) change the shape of the curve, and their coordinates are determined by means of a least-squares (LS) adjustment, where the aim is to minimize the quadratic error between the Cartesian coordinates of the point clouds and the approximated surface. An efficient LS solution is of main importance when statistical tests such as the congruency test are used for deformation detection (Williams *et al*. 2013). Consequently, the variance covariance matrix (VCM) of the measurements has to be specified as accurately as possible (Greene 2003). Dealing with TLS observations, the VCM will thus contain information about the variances of the ranges and angles. Heteroscedasticity can be modelled by means of the datasheet of manufacturers, which give a first indication about the uncertainties of the raw measurements. An improved model was developed for the range variance by means of a power function based on the raw intensity of the reflected objects (Wujanz *et al*. 2017). As the Cartesian coordinates of the CP are needed in a B-spline approximation, the raw observations have to be transformed firstly from polar to Cartesian coordinates, which therefore become correlated. Using the propagation law, the VCM of the transformed coordinates is thus fully populated. Through this manuscript, the term "mathematical correlations" will be used to designate the particular type of correlations due to the transformation from polar to Cartesian coordinates. In contrast, "physical correlations" stem from external (e.g., atmospheric transmission) or sensor internal factors (i.e., within the sensors themselves) and are neglected in this contribution. Indeed, the correlation structure of the measurements remains to be studied more thoroughly as only the residuals of a LS approximation for a plane fitting have been investigated to date (Kauker and Schwieger 2017). Since the transformed diagonal VCM is sparse fully populated, it is questionable whether mathematical correlations could be neglected in the LS adjustment without affecting the results of the test statistics for deformation analysis. In this contribution, we will propose an adapted version of the congruency test (Pelzer 1971) dedicated to surface approximation. We will assess the impact on the derived test statistic of neglecting mathematical correlations up to using only a scaled version of the identity matrix to weight the Cartesian observations. We make use of a real data set of a bridge under loading, where the aim of the experiment was to stress and deform the structure intentionally. Predefined small and deformed surfaces scanned under different geometries were extracted to study the impact of mathematical correlations on the deformation testing approach.

The paper is organised as follows: in section II, the principle of B-spline approximation is presented briefly. We focus specifically on the problem of the stochastic model and the mathematical correlations. Section III is devoted to the case study. We conclude this contribution with some recommendations.

II. MATHEMATICAL BACKGROUND

A. *B-spline surface*

A B-spline surface $\mathbf{s}$ is defined as a network of tensor product B-spline surface patches

$$\mathbf{s}(u,v)=\sum_{i=0}^{n}\sum_{i=0}^{m}N_{i,p}(u)N_{j,q}(v)\mathbf{p}_{i,j} \quad (1)$$

The surface is defined over a given domain with local coordinates $(u,v)\in[0,1]\times[0,1]$. For regularly and rectangular shaped point clouds with s rows and w columns, the chord length method (Piegl and Tiller 1997) is widely employed to determine u and v. $\mathbf{p}_{i,j}$ are the CP or weighting factors of the basis functions $N_{i,p}$ and $N_{j,q}$ of degree p and q respectively. These functions are defined over so-called knot sequences $\mathbf{U}=\begin{bmatrix}u_0 & \dots & u_{n+p+1}\end{bmatrix}, \mathbf{V}=\begin{bmatrix}v_0 & \dots & v_{m+q+1}\end{bmatrix}$ in the u and v direction and can be evaluated by means of a recurrence relationship (Piegl and Tiller 1997; de Boor 2001). In surface reconstruction, one seeks to find the control points such that the distance of the data points to the approximated surface is minimized. To that aim, the minimum in least-squares sense of the zero-mean error term $\mathbf{v}$, defined as the difference between the Cartesian coordinates of the point cloud $\mathbf{l}$ of size *g* and $\mathbf{Ax}$, is searched. $\mathbf{x}$ is the parameter vector to be estimated and $\mathbf{A}$ the deterministic design matrix.

Calling $E(\bullet)$ the expectation operator, we assume $E(\mathbf{l})=\mathbf{Ax}$. If the condition of homoscedasticity of the observations holds, i.e. $\Sigma_{ll}=\sigma_0^2\mathbf{I}$, where Σ_{ll} is the VCM of the observations, σ_0^2 an *a priori* variance factor and $\mathbf{I}$ the identity matrix of size g^2, the estimated coordinates of the control points are expressed by $\hat{\mathbf{x}}_{OLSE}=\left(\mathbf{A}^T\mathbf{A}\right)^{-1}\mathbf{A}^T\mathbf{l}$. This unbiased estimator is called the Ordinary Least-squares Estimator (OLSE, Koch 1999).

The optimal number of control points can be determined using Information Criteria such as BIC or

AIC (Alkhatib *et al*. 2018). Although similar in their formulation, these two criteria are fundamentally different in their philosophy. Whereas BIC is said to be consistent since the data generating model will be selected with growing data size, AIC is efficient and selects the model that predicts the observed data with smallest error. Both criteria may give a different optimum solution. This holds particularly true under model misspecification, e.g., if the data are only poorly approximated by B-splines or if correlations are present. In this contribution, the real data used are unproblematic and correspond to an easy-to-model geometry, so that the results of BIC and AIC agree and are not further discussed. Thus, the functional model of the LS adjustment is considered as optimal.

B. *The generalized least-squares estimator*

Because of the deterministic nature of the design matrix, the unbiasedness of the estimator, expressed as $E(\hat{\mathbf{x}}) = \mathbf{x}$, is not affected by the violation of the condition of homoscedasticity (Kutterer 1999). However, the properties of the OLSE and resulting test statistics are strongly influenced by unequal variances or correlations of the observations (Williams *et al*. 2013). If Σ_{ll} is no longer a scaled identity matrix but becomes fully populated or heteroscedastic, i.e. $\Sigma_{ll} = \sigma_0^2 \mathbf{Q}_0$, with $\mathbf{Q}_0$ defined as the cofactor matrix of the observations, the OLSE is not most efficient within the class of linear unbiased estimators anymore so that hypothesis testing such as the global test or outlier tests becomes invalid. Exemplarily, the *a priori* and *a posteriori* VCM of the estimates defined as follows are biased:

$$\mathbf{Q}_{\mathbf{xx\_OLS}\_apriori} = \sigma_0^2 \left(\mathbf{A}^{\mathbf{T}}\mathbf{A}\right)^{-1} \quad \text{and}$$

$$\mathbf{Q}_{\mathbf{xx\_OLS}\_aposteriori} = \hat{\sigma}_{0\_OLS}^2 \left(\mathbf{A}^{\mathbf{T}}\mathbf{A}\right)^{-1}, \quad \text{where}$$

$\hat{\sigma}_{0\_OLS}^2 = \dfrac{\mathbf{v}^{\mathbf{T}}\mathbf{v}}{r-t}$ is the *a posteriori* variance factor, *t* being the total number of estimated CP. These matrices are unfortunately involved in congruency tests, which are used to detect deformations. As the t and F statistics depend on the elements of these VCM, they no longer have the desired t and F distributions under the null hypothesis that no deformation occurs. Consequently, inference based on these tests is not valid anymore.

When approximating point clouds with B-splines, the assumption of homoscedasticity is common. Indeed, for many applications, obtaining a smoothed approximated surface from scattered point clouds is the main focus, and the computational burden associated with fully populated VCM has to be reduced. In the field of geodesy, however, derived quality indicators turn out to be of major interest since outliers or deformations have to be identified. Consequently, the correct weighting of the observations has a high priority.

As an answer, the Generalized Least-Squares Estimator (GLSE) is thus introduced to improve upon estimation efficiency (Greene 2003). In that case,

$$\hat{\mathbf{x}}_{GLSE} = \left(\mathbf{A}^T\mathbf{P}_0\mathbf{A}\right)^{-1}\mathbf{A}^T\mathbf{P}_0\mathbf{l} \qquad (2)$$

where $\mathbf{P}_0 = \mathbf{Q}_0^{-1}$. The VCM of the estimates is $\mathbf{Q}_{\mathbf{xx\_GLSE}\_apriori} = \sigma_0^2 \left(\mathbf{A}^{\mathbf{T}}\mathbf{P}_0\mathbf{A}\right)^{-1}$ or $\mathbf{Q}_{\mathbf{xx\_GLSE}\_aposteriori} = \hat{\sigma}_0^2 \left(\mathbf{A}^{\mathbf{T}}\mathbf{P}_0\mathbf{A}\right)^{-1}$ with $\hat{\sigma}_{0\_\mathbf{GLSE}}^2 = \dfrac{\mathbf{v}^{\mathbf{T}}\mathbf{P}_0\mathbf{v}}{r-t}$.

Unfortunately, the GLSE cannot be estimated as the true VCM $\mathbf{Q}_0$ can only be estimated by $\hat{\mathbf{Q}}$, e.g. based on expert knowledge. Because in general $\mathbf{Q}_0 \neq \hat{\mathbf{Q}}$, a bias will always remain in the quantity of interest for statistical tests (Kutterer 1999, Kermarrec *et al*. 2017).

Heteroscedasticity

The three measurements of a TLS are (i) the range r expressed in [m], (ii) a vertical and (iii) an horizontal angle called VA and HA respectively, expressed in [°] or [gon]. These quantities have different stochastic properties, which are quantified by their variances σ_r^2, σ_{HA}^2 and σ_{VA}^2. Whereas the angle variance is often assumed to be non-stochastic and is taken constant based on manufacturer datasheet (Boehler and Marbs 2002), σ_r will vary depending e.g. on r, properties of the reflected object and eventually atmospheric transmission (Soudarissanane *et al*. 2011, Zamecnikova *et al*. 2015).

We follow the proposal of Wujanz *et al*. (2017) and model the range variance as depending on the Signal to Noise Ratio (SNR) between the power emitted P_E and received P_R. This quantity measures the strength of the target echo and is also loosely called intensity assuming an extended Lambertian (diffuse) target (Andrews and Phillips 2005). From a theoretical perspective, σ_r can be shown to be proportional to the square root of the SNR (Hebert and Krotkov 1992). Empirically, this dependency was confirmed using the TLS in 1D mode, as well as by residual analysis of plane fitting (Wujanz *et al*. 2017, 2018). The range variance could be fitted with a power function $\sigma_r = c + \beta Int^{\alpha}$, where the parameters α, β and c are determined empirically by regression analysis for different laser scanners and Int is the raw intensity expressed in [Inc]. For the TLS Z+F 5006H under consideration in our case study, we assume a standard deviation of 7° root mean square for both angles as well as $[\alpha, \beta, c] = [-0.57, 1.6, 0]$. For a mean raw intensity of 930000 Inc for the selected

surfaces, σ_r reaches thus in mean 0.64 mm. This value is close to the one given by the manufacturer datasheet (0.7 mm for a reflectivity at 20% corresponding to grey reflected objects scanned at 10 m distance) and is thus plausible and coherent.

We further adopt the strategy proposed by Kermarrec *et al*. (2018) to simplify the stochastic description of the range and avoid a point-wise weighting. Based on a sensitivity analysis of the coefficients of the intensity model, we replace σ_r by a global value, which is computed using the mean of the intensity values of the object, i.e.

$$\sigma_{r,mean} = \beta(\overline{Int})^{\alpha} \quad (3)$$

where $\overline{Int}$ is the mean of the intensities of the reflected object. This simplification holds true for objects having homogeneous properties, i.e. the intensity values should not vary sharply due to e.g. challenging scanning geometries. Because we approximate small surfaces of a continuous object (a bridge), the corresponding conditions are met.

The stochasticity of the TLS measurements are resumed in a matrix form:

$$\hat{\boldsymbol{\Sigma}} = \begin{bmatrix} \hat{\boldsymbol{\Sigma}}_{\mathrm{r}} & 0 & 0 \\ 0 & \hat{\boldsymbol{\Sigma}}_{\mathrm{HA}} & 0 \\ 0 & 0 & \hat{\boldsymbol{\Sigma}}_{\mathrm{VA}} \end{bmatrix} = \sigma_0^2 \hat{\mathbf{Q}}_{without\_MC} \quad (4)$$

where the block matrices $\hat{\boldsymbol{\Sigma}}_{\mathrm{r}}, \hat{\boldsymbol{\Sigma}}_{\mathrm{HA}}, \hat{\boldsymbol{\Sigma}}_{\mathrm{VA}}$ are sorted point-wise and their diagonal elements are given by the corresponding variances $\sigma^2_{r\_mean}, \sigma^2_{HA}, \sigma^2_{VA}$. $\hat{\mathbf{Q}}_{without\_MC}$ is the cofactor matrix before taking mathematical correlation (MC) into account.

Mathematical correlations

Contrary to a plane fitting using a Gauss-Helmert-Model (cf. Wujanz *et al*. 2017), B-spline approximation involves the Cartesian coordinates of the point clouds. A transformation from the raw TLS measurements expressed in polar to the mandatory Cartesian coordinates is thus necessary. The VCM $\hat{\mathbf{Q}} = \hat{\mathbf{Q}}_{MC}$ of the Cartesian coordinates of the point cloud is obtained by the error propagation law:

$$\hat{\mathbf{Q}}_{MC} = \mathbf{F}\hat{\mathbf{Q}}_{without\_MC}\mathbf{F}^{\mathrm{T}} \quad (5)$$

The matrix $\mathbf{F}$ contains the derivatives of the point coordinates with respect to the range and angles and reads for one point *i*:

$$\mathbf{F}_i = \begin{bmatrix} \sin(VA_i)\cos(HA_i) & r_i\cos(VA_i)\cos(HA_i) & -r_i\sin(VA_i)\sin(HA_i) \\ \sin(VA_i)\sin(HA_i) & r_i\cos(VA_i)\sin(HA_i) & r_i\sin(VA_i)\cos(HA_i) \\ \cos(VA_i) & -r_i\sin(VA_i) & 0 \end{bmatrix} \quad (6)$$

As a consequence, the corresponding "Cartesian" variances for one point of the point clouds are:

$$\sigma_X^2 = (r\cos HA\cos VA)^2\sigma_{HA}^2 + (r\sin HA\sin VA)^2\sigma_{VA}^2 + (\cos HA\sin VA)^2\sigma_r^2$$
$$\sigma_Y^2 = (r\sin HA\cos VA)^2\sigma_{HA}^2 + (r\cos HA\sin VA)^2\sigma_{VA}^2 + (\sin HA\sin VA)^2\sigma_r^2$$
$$\sigma_Z^2 = (r\sin VA)^2\sigma_{HA}^2 + (\cos HA)^2\sigma_r^2 \quad (7)$$

The subscript *i* is skipped for the sake of readability. The Cartesian coordinates become unfortunately mathematically correlated and the corresponding covariances read:

$$\sigma_{XY}^2 = \sigma_{YX}^2 = (\cos HA\sin HA\sin^2 VA)\sigma_r^2 + \ldots$$
$$(r^2\cos HA\sin HA\cos^2 VA)\sigma_{HA}^2 - (r^2\sin HA\cos HA\sin^2 VA)\sigma_{VA}^2$$
$$\sigma_{XZ}^2 = \sigma_{ZX}^2 = (-r^2\cos HA\sin HA\cos VA)\sigma_{HA}^2 + (\cos HA\sin VA\cos VA)\sigma_r^2$$
$$\sigma_{YZ}^2 = \sigma_{ZY}^2 = (-r^2\sin HA\cos VA\sin VA)\sigma_{HA}^2 + (\sin HA\sin VA\cos VA)\sigma_r^2 \quad (8)$$

Fully populated VCM increase the computational burden, particularly when a huge amount of points has to be approximated. We therefore propose to investigate if mathematical correlations can be neglected or even replaced by a constant scaling factor, following the proposal of Kermarrec and Schön (2016) for physical correlations. To that end, we study in a first step the behaviour of the ratios of the covariances to the corresponding variances, i.e. $R_X = \left[\sigma^2_{XY}/\sigma^2_X, \sigma^2_{XY}/\sigma^2_Y, \sigma^2_{XY}/\sigma^2_Z \right]$, $R_Y = \sigma^2_{XZ}/\sigma^2_X, \sigma^2_{XZ}/\sigma^2_Y, \sigma^2_{XZ}/\sigma^2_Z$ and $R_Z = \sigma^2_{YZ}/\sigma^2_X, \sigma^2_{YZ}/\sigma^2_Y, \sigma^2_{YZ}/\sigma^2_Z$. Two cases are considered: (i) an object situated at a range of 10 m, for which a range standard deviation of 0.7 mm is assumed following the manufacturer's datasheet and (ii) in a second case, an object at a distance of 25 m, with a corresponding range standard deviation of 7 mm. We aim to investigate how R_X, R_Y, R_Z behaves depending on the ratio σ^2_r/σ^2_{HA}. The corresponding results are presented in Figure 1, where we restrict ourselves for the sake of shortness to R_X. The VA and HA are varied in a range from 0° to 90°. Other combinations can be obtained per symmetry from Eq. (7) and Eq. (8).

In Figure 1 (top), we see that the ratios are under 1, even under 0.1 for most of the geometries, i.e. combinations of VA and HA. Consequently, the covariances are more than 10 times smaller than the variances. Neglecting the cross diagonal elements thus seems plausible. Under unfavourable geometries, however, it happens that the covariances become large. This situation occurs mostly when the angles are close to 0 or 90°. In such extreme scanning situations, other effects such as physical correlations may additionally affect the covariances of the raw observations, which is the topic of further studies. In Figure 1 (bottom), the range is increased, i.e. its standard deviation is larger accordingly. Consequently, the ratios under consideration have a stronger variability with higher values for a lager range of angles, compared with the one presented in Figure 1 (top). This would lead to a

stronger effect at the level of test statistics when mathematical correlations are neglected.

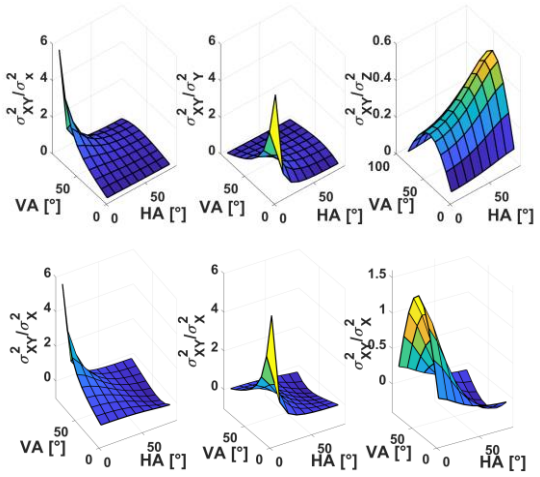

Figure 1. Ratio R_X (top) for a range of 7 m and a corresponding range standard deviation of 0.0007 m and (bottom) for a range of 25 m and a corresponding range standard deviation of 0.007 m

C. *Congruency test for B-splines approximation*

To test for deformation between a first (1) and a second (2) epoch, we make use of an adapted form of the global congruency test as derived by (Pelzer 1971). This adaptation is made necessary since the deformation is not tested at the parameter level but rather at the level of the estimated surfaces. The surface points at a given epoch are estimated by a matrix product $\mathbf{Fx}$ from Eq. (1). After determining the stochastic and the functional model of the B-spline approximation, the uniformly most powerful invariant test for deformation can be shown to be based on the test statistic:

$$T_{apriori} = \hat{\boldsymbol{\Delta}}^{\mathrm{T}}\boldsymbol{\Sigma}^{-1}_{\hat{\boldsymbol{\Delta}}\hat{\boldsymbol{\Delta}}}\hat{\boldsymbol{\Delta}} = \frac{1}{\sigma_0^2}\hat{\boldsymbol{\Delta}}^{\mathrm{T}}\mathbf{Q}^{-1}_{\hat{\boldsymbol{\Delta}}\hat{\boldsymbol{\Delta}}}\hat{\boldsymbol{\Delta}} \sim \chi^2_p \quad (9)$$

$$\boldsymbol{\Sigma}_{\hat{\boldsymbol{\Delta}}\hat{\boldsymbol{\Delta}}} = \mathbf{H}\boldsymbol{\Sigma}_{\hat{\boldsymbol{\beta}}\hat{\boldsymbol{\beta}}}\mathbf{H}^{\mathrm{T}}$$

where $\boldsymbol{\Sigma}_{\hat{\boldsymbol{\beta}}\hat{\boldsymbol{\beta}}}$ is the VCM of the estimated CP for both epochs and $\hat{\boldsymbol{\beta}} = \begin{bmatrix} \hat{\mathbf{x}}_{\mathbf{epoch1}} \\ \hat{\mathbf{x}}_{\mathbf{epoch2}} \end{bmatrix}$ contains the LS estimates of the CP. $\mathbf{H}$ is split in two parts to build a difference at the level of the surface points: $\mathbf{H} = \begin{bmatrix} -\mathbf{F}_{\mathbf{epoch1}} & \mathbf{F}_{\mathbf{epoch2}} \end{bmatrix}$ with p rows.

The *a posteriori* test statistic is derived similarly by replacing the apriori variance σ_0^2 by the *a posteriori* counterpart $\hat{\sigma}_0^2$. In that case, however, $T_{aposteriori}$ follows an F-distribution (Teunissen 2000).

The null hypothesis H_0 states that no deformation occurs, i.e. $\boldsymbol{\Delta} = 0$, where the estimate of the deformation or difference between the two surfaces is given by $\hat{\boldsymbol{\Delta}} = \mathbf{H}\hat{\boldsymbol{\beta}}$. The alternative hypothesis H_1 is $\boldsymbol{\Delta} \neq 0$. The test decision involves the quantile $k^{\chi^2_p}_{1-\alpha}$ based on the χ^2_p test distribution and the significance level α. In particular, H_0 is accepted if $T_{apriori} \leq k^{\chi^2_p}_{1-\alpha}$.

Clearly, the test statistics $T_{apriori}$ or $T_{aposteriori}$ involve the VCM of the CP estimates $\mathbf{Q}_{\mathbf{xx\_GLSE}\_apriori}$ and $\mathbf{Q}_{\mathbf{xx\_GLSE}\_aposteriori}$, respectively, through $\boldsymbol{\Sigma}_{\hat{\boldsymbol{\beta}}\hat{\boldsymbol{\beta}}}$. As a consequence, the VCM of the underlying observations $\hat{\mathbf{Q}} = \hat{\mathbf{Q}}_{MC}$ plays a crucial role in detecting a deformation or not: neglecting mathematical correlations can potentially cause a too small $T_{apriori}$ or $T_{aposteriori}$. This situation may arise when the Euclidian norm of the surface differences between 2 epochs $\left\|\hat{\boldsymbol{\Delta}}\right\|$ is small so that the subtle effect of accounting for the VCM $\boldsymbol{\Sigma}_{\hat{\boldsymbol{\Delta}}\hat{\boldsymbol{\Delta}}}$ can be decisive, variations of $T_{apriori}$ or $T_{aposteriori}$ around the quantile leading potentially to a non-detection of existing deformation, i.e. wrong acceptance of H_0. Due to the unbiasedness of the GLSE when enough point clouds are processed, changing the VCM of the observations does not lead to strong differences in estimating $\hat{\boldsymbol{\Delta}}$ (Kutterer 1999). However, some care is needed when scaling the VCM used in the comparison. In this contribution, we will focus on three versions of $\hat{\mathbf{Q}}$: $\hat{\mathbf{Q}}_{MC}, \hat{\mathbf{Q}}_{MC\_diag} = diag\left(\hat{\mathbf{Q}}_{MC}\right), \sigma^2_{scaled}\mathbf{I}$. The matrix $\hat{\mathbf{Q}}_{MC}$ accounts both for the heteroscedasticity of the observations and the mathematical correlations and has a block diagonal structure. $\hat{\mathbf{Q}}_{MC\_diag}$ contains only the diagonal elements of $\hat{\mathbf{Q}}_{MC}$, i.e. the correlations are neglected. $\sigma^2_{scaled}\mathbf{I}$ is a scaled version of the identity matrix. σ^2_{scaled} is determined by taking the mean of the diagonal elements of $\hat{\mathbf{Q}}_{MC\_diag}$ over all points. The scaling is necessary for the sake of comparison between matrices as the VCM is only involved once in Eq. (9). Obtaining similar results with all three matrices would indicate that a simplification with an easy to handle identity matrix can be considered under the uncertainty model chosen. When dealing with deformations, we prefer an inadequate acceptance of the alternative hypothesis H_1. As the surfaces under consideration in the following case study are small, we do not carry out local congruency tests on specific points, which would

have further the disadvantage of being more strongly influenced by small variations of the estimated surfaces due to the stochastic model, making comparisons of the test statistics difficult in view of their strong variability.

III. CASE STUDY

A. *Description of the data set*

In this section, we use a real data set of an historic masonry arch bridge over the river Aller near Verden in Germany to compare the results of the test statistics for detecting deformation at the level of the B-spline approximation. The TLS observations stem from an experiment carried out in the framework of the interdisciplinary project "Application of life cycle concepts to civil engineering structures" (Schacht *et al*. 2017). In order to simulate the deformation, loads of increasing weights were artificially added on specific parts of the bridge to simulate the impact induced, e.g., by car traffic. 2D profiles were captured using a Zoller+Fröhlich Imager 5006H at a sampling rate of 500,000 points per second. Objects such as prisms were removed from the obtained data set. After a data gap handling and a projection of the 3D point cloud onto a regular grid, the B-spline approximation of the arch bridge was performed.

Using a specific software (CloudCompare), six surfaces were selected for deformation analysis. Their surface area is approximately 0.05 m^2. The grid size was chosen such that for all cases 300 +/-25 points were taken into account. Their localisation on the complete bridge and their identification number are shown in Figure 2. Four epochs were considered for further analysis: the first one corresponds to the reference (no load), whereas the fourth one corresponds to the maximum load, i.e. maximum deformation. As the weights were applied to the middle of the bridge, we expect zones 1-3 to be more influenced by the loading than zones 4-6, which are situated near the extremity of the bridge on the right side (see Table 1, last row).

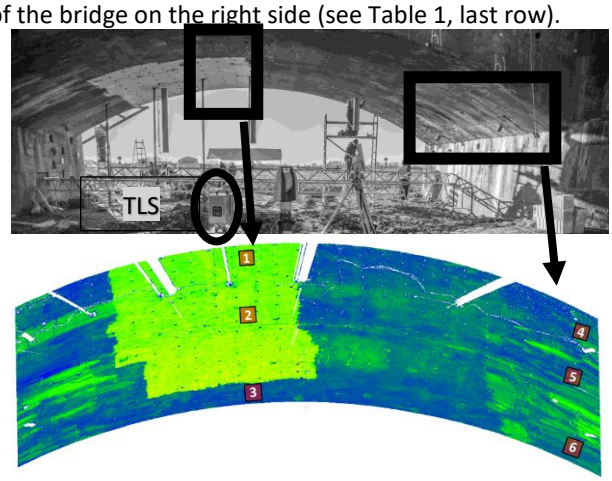

Figure 2. top: historic bridge and bottom: representation in CloudCompare with position of the six surfaces under consideration for deformation analysis (from Paffenholz et al. 2018)

B. *Results*

We performed an approximation of the surfaces using B-splines as presented in Section II. The optimal number of CP was fixed by means of the BIC and AIC, which agreed to an optimal number of 9 CP, i.e., 3 CP in each direction. The global test was carried out to check for misspecification in each case under consideration. The mean raw intensity values were integrated in the stochastic model (3) to compute the range variances. Table 1 summarizes the mean properties of the different surfaces, including the scanning geometry. In Table 1, we additionally give $\left\|\hat{\Delta}\right\|$, which is the Euclidian norm of the estimated surface differences in [m] with respect to the reference to assess the amplitude of the expected deformation for the 4 cases, i.e. between epoch 0-1, 0-2, 0-3 and 0-4, where 0 corresponds to the reference epoch (no deformation).

Zone	1	2	3	4	5	6
HA [°]	1.5-3	2.2-4	4.3-10.6	100.6-101.7	102.9-104.1	106-107.7
VA [°]	110-111	119-120	146.6-150	318.6-321	309-311	287.5-290
Range [m]	8.9-9.1	6.4-6.6	3.79-3.95	10.8-11.2	9.2-9.5	7.5-7.8
$\left\|\hat{\Delta}\right\|$						
0-1	0.051	0.034	0.015	0.018	0.016	0.009
0-2	0.093	0.065	0.025	0.021	0.014	0.007
0-3	0.145	0.101	0.042	0.017	0.017	0.008
0-4	0.198	0.140	0.054	0.021	0.021	0.008

Table 1: properties of the six surfaces

The quantile of the tests depends on the parameter α chosen, which is thus the decision of the user. In this contribution, we focus on the behaviour of $T_{apriori}$ when the VCM of the observations is varied. As $T_{aposteriori}$ led to the same conclusions, we do not present the corresponding results for the sake of shortness. The corresponding results for $T_{apriori}$ for the six surfaces under consideration (Figure 2) are presented in Figure 3 (left) and (right) for the four deformation scenarios.

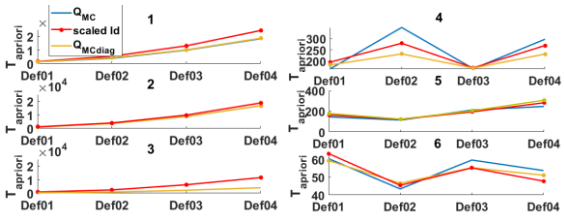

Figure 3. $T_{apriori}$ for the six surfaces: left zone 1-3 and right zone 4-6. Four deformation scenarios corresponding to an increased magnitude are named Def01, Def02, Def 03 and Def04 for "Deformation between epoch 0 and 4".

From Figure 3, a clear difference can be identified regarding the impact of neglecting mathematical

correlations (blue and yellow lines). For the first three surfaces where a strong deformation occurs, the differences between $T_{apriori}$ computed with $\hat{\mathbf{Q}}_{MC}$, $\hat{\mathbf{Q}}_{MC\_diag}$ are negligible for all deformation cases. Exemplarily, for zone 3, it reaches the value of 3 for Def01 and 25 for Def04. Because $T_{apriori}$ is far below the critical value for $\alpha = 0.05$, this small difference has no impact on the rejection of the null hypothesis. By comparing the angle and range values of Table 1 for zone 1-3 with Figure 2, we additionally point out that the geometry of the scans correspond to cases where the ratio R_X was far under 1. For these specific configurations, the mathematical correlations can thus be neglected. The scaled identity matrix is a possible alternative, although it would lead here to an overestimation of $T_{apriori}$ because of the aforementioned small influence of the mathematical correlations. The overestimation remains better than an underestimation, i.e. the non-detection of deformation. However, for the zones 4-6, which are much less strongly impacted by the loading (Table 2) than zones 1-3, the impact of the scaled identity and $\hat{\mathbf{Q}}_{MC\_diag}$ on $T_{apriori}$ is slightly different. Differences between $T_{apriori}$ for $\hat{\mathbf{Q}}_{MC}$ and $\hat{\mathbf{Q}}_{MC\_diag}$ of up to 70 can be obtained, which could be, with regard to the small deformation, critical. Indeed, the approximated matrices lead to an underestimation of $T_{apriori}$. The reason for this behaviour is related both (i) to the small deformation magnitude under consideration, as well as (ii) to the unfavourable scanning geometry. Because HA and VA reach the values of approximately 100° and 300°, a deeper analysis of Figure 1 (top) highlights a strong increase of the ratio R_X. Additionally, the range is larger and the intensity values lower due to the scanning condition, so that R_X tends to be comparable to the shape found in Figure 1 (bottom). Consequently, mathematical correlations should not be neglected under unfavourable scanning geometries.

For scanned objects with mean HA and VA between 20° and 80°, mathematical correlations can be neglected due to averaging effects, and a simplified stochastic model can be used. The same holds true when deformation are large. However, when extremely small deformations are suspected (under 1 mm), the most accurate VCM should be preferred so that the congruency test can reach its optimal efficiency.

IV. CONCLUSIONS

The detection of deformation from TLS observations can be done either at the point cloud level or at the level of an approximated surface. This geometry-based strategy compares approximated analytic functions, i.e. cylinder, planes or free-form curves from different epochs. The B-spline surface approximation has been shown to provide a good balance between complexity and accuracy, and is increasingly used to model objects scanned by TLS. An LS adjustment is performed to determine the coordinates of CP that determine the shape of the final surfaces. To reach the best efficiency of the LS estimator, the weighting with the true VCM of the observations is indispensable. The heteroscedasticity of TLS range measurements can be modelled based on the SNR or equivalently intensity values, and depends thus on the scanned objects and the geometry. Angles are assumed to have a constant variance taken from the manufacturer's datasheet. As B-spline approximations have to be performed with Cartesian coordinates, a transformation of the VCM is needed to account for mathematical correlations. Since a resulting fully populated VCM is less easy to handle than a diagonal VCM, we investigated in which cases such correlations can be neglected. It could be shown exemplarily that the magnitude of the cross diagonal elements of the VCM of the transformed observations in comparison to the diagonal elements increases under unfavourable geometries, i.e. mostly for small horizontal and vertical angles, angles close to 90°, and higher ranges. A case study corresponding to a deformed bridge under loading confirmed this dependency by analysing the value of an adapted version of the congruency test statistic for approximated surfaces to detect deformations. We have shown that for small deformations under unfavourable geometries, neglecting mathematical correlations should be avoided, i.e. differences around 30-50 for the *a priori* test statistics were found. For larger objects with an average geometry, either a scaled identity matrix or the diagonal version of the fully populated VCM accounting for mathematical correlations can be used. However, this simplification is to be taken with caution, particularly when the estimated standard deviation of the range increases with respect to the one chosen for the angles. In this contribution, we focused on mathematical correlations. The conclusions are similar for other sensors which measurements are made in polar coordinates and the post processing implies a coordinate transformation. The impact of additional temporal correlations remains to be further studied since their structure will similarly affect the test statistics, see Kermarrec et al. (2019) for a parallel between the expected correlations of TLS and GNSS range observations.

References

Alkhatib, H.; Kargoll, B.; Bureick, J.; Paffenholz, J.A. (2018) Statistical evaluation of the B-Splines approximation of 3D point clouds. In *Proceedings of the 2018 FIG-Congress,* Istanbul, Turkey, 6–11 May 2018.

Andrews, L.C.; Phillips, R.L. (2005) *Laser Beam Propagation through Random Media*, 2nd ed.; *SPIE—The International*

Society for Optical Engineering: Washington, DC, USA, 2005.

Boehler, W.; Marbs, A. (2002) A. 3D Scanning instruments. *In Proceedings of the CIPA WG6 International Workshop on Scanning for Cultural Heritage Recording*, Corfu, Greece, 1–2 September 2002.

Bureick, J.; Alkhatib, H.; Neumann, I. (2016) Robust spatial approximation of laser scanner points clouds by means of free-form curve approaches in deformation analysis. *J. Appl. Geod.* 10, 27–35.

Caspary, W. F. (1987). Concept of Network and Deformation Analysis. School of Surveying, The University New South Wales, Monograph 11.

de Boor, C.A. (2001) Practical Guide to Splines, Revised ed.; Springer: New York, NY, USA, 2001.

Gálvez, A.; Iglesias, A.; Avila, A.; Otero, C.; Arias, R.; Manchado, C. (2015) Elitist clonal selection algorithm for optimal choice of free knots in B-spline data fitting. Applied Soft Computing 26, 90–106.

Greene, W.H. (2003) Econometric analysis, 5th ed.; PrenticeHall: Upper Saddle River, NJ, USA, 2003.

Gumus, K.; Erkaya, H; Soycan, M. (2013) Investigation of repeatability of digital surface models obtained from point clouds in a concrete arch dam for monitoring of deformations. *Boletim Geodesicas de Ciencias*, 19, 268-286.

Hebert, M.; Krotkov, E. (1992) 3D measurements from imaging laser radars: How good are they? *Image Vis. Comput.* 10, 170–178.

Kauker, S.; Schwieger, V. (2017) A synthetic covariance matrix for monitoring by terrestrial laser scanning. A synthetic covariance matrix for monitoring by terrestrial laser scanning. *J. Appl. Geod.* 11, 77–87.

Kermarrec, G.; Schön, S. (2016) Taking correlation into account with a diagonal covariance matrix. *J. Geod.* 90, 9, 793-805.

Kermarrec, G.; Schön, S. (2017) A priori fully populated covariance matrices in Least-Squares adjustment—Case Study: GPS relative positioning. *J. Geod.* 91, 465–484.

Kermarrec, G.; Alkhatib H.; Neumann I. (2018) On the Sensitivity of the Parameters of the Intensity-Based Stochastic Model for Terrestrial Laser Scanner. Case Study: B-Spline Approximation. Sensors, 18, 2964.

Kermarrec G.; Neumann I.; Alkhatib H.; Schön S. (2019) The stochastic model for Global Navigation Satellite Systems and terrestrial laser scanning observations: a proposal to account for correlations in least squares adjustment. *J. Appl. Geod.* Retrieved 19 Feb. 2019, from doi:10.1515/jag-2018-0019

Koch, K.R. (1999) Parameter Estimation and Hypothesis Testing in Linear Models; Springer: Berlin, Germany, 1999.

Koch, K. R. (2009) Fitting free-form surfaces to laserscan data by NURBS. *AVN Allg. Vermess.-Nachr.* 116, 134–140.

Kutterer, H. (1999) On the sensitivity of the results of least-squares adjustments concerning the stochastic model. *J. Geod.* 73, 350–361.

Lenzmann, L.; Lenzmann, E. (2004) Strenge Auswertung des nichtlinearen Gauß Helmert-Modells. *AVN Allg. Vermess.-Nachr.* 111, 68–73.

Paffenholz, J.-A.; Bae, K.-H. (2012) Geo-referencing point clouds with transformational and positional uncertainties, *J. Appl. Geod.* 6, 33–46.

Pelzer, H. (1971) Zur analyse geodatischer deformations-messungen., Munchen, Verlag der Bayer. Akad. d. Wiss; Munchen, Beck400 [in Komm.] 1971. 164

Pesci, A.; Teza, G.; Bonali, E.; Casula G.; Boschi, E. (2013) A laser scanning-based method for fast estimation of seismic-induced building deformations. *ISPRS J Photogrammetry Remote Sens*, 79, 185-198

Piegl, L.; Tiller, W. (1997) The NURBS Book; Springer Science & Business Media: Berlin, Germany, 1997

Schacht, G.; Piehler, J.; Müller, J.Z.A.; Marx, S. (2017) Belastungsversuche an einer historischen Eisenbahn-Gewölbebrücke. *Bautechnik* 94, 125–130.

Soudarissanane, S.; Lindenbergh, R.; Menenti, M.; Teunissen, P. (2011) Scanning geometry: influencing factor on the quality of terrestrial laser scanning points. *ISPRS 2011*, 66, 389-399

Teunissen, P.J.G. (2000) Testing Theory; An Introduction; *VSSD Publishing: Delft*, The Netherlands, 2000.

Williams, M.N.; Gomez Grajales, C.A.; Kurkiewicz, D. (2013) Assumptions of Multiple Regression: Correcting Two Misconceptions. Practical Assessment. *Res. Eval.* 18, 11.

Wujanz, D.; Burger, M.; Mettenleiter, M.; Neitzel, F. (2017) An intensity-based stochastic model for terrestrial laser scanners. *ISPRS J. Photogramm. Remote Sens.* 125, 146–155.

Wujanz, D.; Burger, M.; Tschirschwitz, F.; Nietzschmann, T.; Neitzel, F.; Kersten T.P. (2018) Determination of intensity-based stochastic models for terrestrial laser scanners utilising 3D-point clouds. *Sensors* 18, 2187.

Yang, H.; Xu, X.; Xu, W.; Neumann, I. (2017) Terrestrial laser scanning-based deformation analysis for arch and beam structures. *IEEE Sens. J.* 17, 4605-4611

Zámečníková, M.; Neuner, H.; Pegritz, S.; Sonnleitner, R. (2015) Investigation on the influence of the incidence angle on the reflectorless distance measurement of a terrestrial laser scanner. *Österr. Z. Vermess. Geoinform.* 103, 208–218.